Journal of Materials Chemistry C

Accepted Manuscript

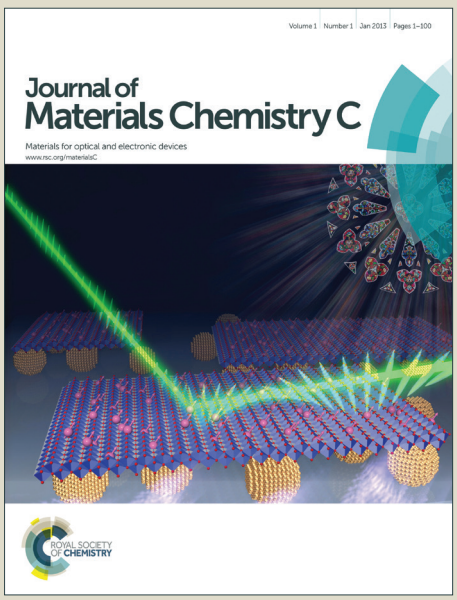

ROYAL SOCIETY OF CHEMISTRY

www.rsc.org/materialsC

Cite this: DOI: 10.1039/c0xx00000x

www.rsc.org/xxxxxx

ARTICLE TYPE

Investigations on PVP/Y_3BO_6:Eu^{3+}, a red luminescent composite for lighting devices based on near UV-LEDs

Nathalie Pradal,[a,b] Damien Boyer,[a,b] Geneviève Chadeyron, *[,a,b] Sandrine Therias,[b,c] Anthony Chapel,[b,c] Celso V. Santilli,[d] and Rachid Mahiou, [b,c]

Received (in XXX, XXX) Xth XXXXXXXXX 20XX, Accepted Xth XXXXXXXXX 20XX
DOI: 10.1039/b000000x

This work deals with a red phosphor, Y_3BO_6:Eu^{3+}, and its corresponding Poly(N-vinylpyrrolidone) (PVP)/Y_3BO_6:Eu^{3+} luminescent composite film suitable for applications in a next generation of Hg-free lamps based on near ultraviolet (UV) light emitting diodes (LEDs). Well crystallized samples of Y_3BO_6 powders with Eu^{3+} content up to 20 mol% were prepared by Pechini method. After structural, morphological and optical characterizations, the best doping rate of Eu^{3+} in the matrix was determined to be 15 mol%. This optimal powder, which is highly friable, was easily grinded into fine particles and homogeneously dispersed into a PVP polymer solution to give rise to a polymer phosphor composite. Structural and optical features of the composite film have been studied and compared to those of a pristine PVP film and Y_3BO_6:Eu^{3+} powder. All the characterizations (XRD, SAXS, luminescence…) proved that the red phosphor particles are well incorporated into the polymer composite film which exhibited the characteristic red emission of Eu^{3+} under UV light excitation. Furthermore, photostability of the polymer/phosphor composite film under UV-LED irradiation was evaluated from exposure to accelerated artificial photoageing at wavelengths above 300 nm.

Introduction

For the coming years, most of white light emitting devices will be based on light emitting diodes (LEDs) combined with suitable phosphors. The LEDs technology is considered to be eco-friendly since it prevents the use of mercury like in fluorescent lamps and it consumes much less energy in comparison with incandescent lamps[1]. Up to now, the common approach for producing white-emitting LEDs has consisted in combining a blue-emitting InGaN LED (λ_{ex} = 465 nm) with a yellow phosphor $Y_3Al_5O_{12}$:Ce^{3+} (YAG:Ce) and a red emitting phosphor for color correction[2-3]. However a new strategy based on near UV-LED is being investigated. Indeed, the combination of a near UV-LED with three phosphors (red, green and blue) is expected to enable a better control over color rendering index and color temperature[4-5]. In most cases, to be associated with a LED, these phosphors must be incorporated in a polymer matrix resulting in luminescent composites[6-8].

Lanthanides borates have already been evidenced to be relevant candidates in optical devices as red-emitting phosphor when doped with Eu^{3+} ions. In addition to high thermal stability, this class of luminescent materials exhibit high quantum efficiency upon UV excitation[9-11].

In this work, we have focused our attention on Y_3BO_6:Eu^{3+}, which was already synthesized by the sol-gel process in our group[12], since this phosphor exhibits excellent chromaticity coordinates for a red component (x=0.64; y=0.33). Well crystallized samples of Y_3BO_6 powders with Eu^{3+} content up to 20 mol% (not reached by the sol-gel process) were prepared by a new synthesis way based on the Pechini method[13].

These powders were incorporated into a Poly(N-vinylpyrrolidone) (PVP) polymer with a loading rate of 20 wt% in order to achieve luminescent composite films. PVP was used as a model polymer because of its characteristics such as its solubility in eco-friendly solvents (such as alcohols and water), it does not absorb in the visible range[14] and the photochemical behavior of PVP films under UV-light irradiation is well-known[15].

After structural and morphological characterizations, the best doping rate of Eu^{3+} in Y_3BO_6 powders was determined. Afterwards, the optical properties were studied before and after incorporation in the PVP matrix. Furthermore, the influence of the PVP degradation on the luminescent properties of the composite was investigated.

Experimental Section

Materials

Poly(N-vinylpyrrolidone) (PVP) sample was supplied by Scientific Polymer Products. The average molar weight of the polymer was 360000 $g.mol^{-1}$.

$Y(NO_3)_3.6H_2O$ (purity 99.9+%), $Eu(NO_3)_3.6H_2O$ (purity 99.9+%) and citric acid (CA - purity 99+%) were obtained from

Aldrich whereas H_3BO_3 (purity 99+%) and PEG 200 were purchased respectively from Prolabo and Sigma-Aldrich.

Preparation of Eu^{3+}-doped Y_3BO_6

Eu^{3+}-doped Y_3BO_6 powders were prepared by Pechini method. The detailed procedure can be described as follows[10]:

(1) $Y(NO_3)_3.6H_2O$, $Eu(NO_3)_3.6H_2O$ and H_3BO_3 were added to a water-ethanol solution (the volume ratio was 1:4) under stirring. Metal nitrates were weighed stoichiometrically whereas a 40 mol% excess of H_3BO_3 was used because a part of the boron atoms is volatilized during the steps of heating.

(2) Citric acid and PEG 200 were added to the above solution with a molar ratio H_3BO_3:CA:PEG = 5.5:15:1. The citric acid and PEG were used as the chelating and cross-linking reagents, respectively.

(3) The above solution was stirred for 5 hours at room temperature in order to form a sol. This sol was dried at 80°C for about 12 hours to give a xerogel.

(4) After preheating the xerogel at 400°C for 2 hours in air atmosphere, the samples were grounded and heated at 1000°C for 4 hours in air. For each treatment, the heating rate is fixed at 5°C.min^{-1}.

The whole process resulted into a foamy white powder with a red emission under UV excitation. Powders were then grounded as finely as possible in an agate mortar in order to achieve the different characterizations. Different concentrations of Eu^{3+} in Y_3BO_6 (1, 3, 5, 10, 15 and 20 mol%) were achieved in order to determine the optimal concentration leading to the best optical properties upon UV excitation.

Elaboration of PVP/Y_3BO_6:Eu^{3+} composite films

$Y_{2.55}Eu_{0.45}BO_6$ powder was used to elaborate the polymer/phosphor composite since (seen paragraph 3) 15 mol% has been determined as the optimal concentration.

Polymer/phosphor composite films were prepared from a solution using a film casting method. PVP powder was dissolved in isopropanol (83.3 g.L^{-1}) under mild heating conditions. Then, appropriate amount of $Y_{2.55}Eu_{0.45}BO_6$ powder was incorporated into PVP solution in order to obtain a phosphor loading rate of 20 wt%. Thereafter a step of sonication for 10 min with an ultrasonic probe (Sonics Vibra-cell 130W) was applied in order to obtain a well dispersed mixture. This loading rate of 20 wt% was chosen in reason of previous study carried out in our laboratory: it leads to a good compromise to obtain both suitable mechanical and optical properties. The composite solution was deposited onto Teflon sheets by means of an Erichsen Coatmaster 809 MC (knife height was 400 µm, casting speed 20 mm.s^{-1}). Films were obtained after drying at 40°C for 10 min, and few hours at room temperature. Free-standing films with thickness about 30 µm were then obtained and used for further analyses.

Irradiation of films

UV-visible light irradiation (λ>300 nm) of the films in presence of oxygen was performed in a SEPAP 12-24 unit (ATLAS), which was designed for studying polymer photodegradation under artificial ageing conditions[16]. These conditions of irradiation are those of natural outdoor aging but were chosen to simulate the UV-LED irradiation. The chamber consisted of a square reactor equipped with four medium-pressure mercury lamps (Novalamp RVC 400W) situated vertically at each corner of the chamber. Wavelengths below 300 nm are filtered by the glass envelope of the lamps. In the centre of the chamber, the samples were fixed on a rotating carousel. The temperature at the sample surfaces was set to 60°C, controlled by a thermocouple.

Characterization techniques

X-Ray Diffraction. High-Temperature X-Ray Diffraction (HTXRD) analyses were performed on a Philips X-Pert Pro diffractometer operating with the Cu-Kα radiation (λ=1,5406Å) and equipped with a high-temperature chamber, over a temperature lying from 25 to 1000°C in air atmosphere. A sequential temperature rising rate of 5°C.min^{-1} and 1 hour temperature holding time prior to each measurement were used. Temperature was determined by means of Pt/Pt-Rh thermocouple. XRD patterns were recorded on the same diffractometer operating with the Cu-Kα radiation.

Thermogravimetric and differential thermal analyzes. TG and DTA measurements were performed on a SETARAM Setsys Evolution 1750 thermogravimetric analyzer. The samples were heated in air between 25 and 1000°C at a rate of 5°C.min^{-1}.

Infrared Spectroscopy. Infrared transmission spectra of composites were recorded using a Nicolet 760-FTIR spectrometer with OMNIC software. Spectra were obtained using a summation of 32 scans and a resolution of 4 cm^{-1}. A calibration of the thickness (e, µm) of the non-photooxidized samples was performed by measuring the absorbance (OD) at 1370 cm^{-1}, which corresponds to a vibration band of the (C–H) bending mode. The thickness (e) dependence of the absorbance obeyed the equation OD=0.0175 x e[15]. In the case of powders, infrared transmission spectra were recorded on a Thermo-Nicolet 5700 spectrometer using the KBr pellet technique.

Raman Spectroscopy. Raman spectra were recorded using a T64000 Jobin-Yvon confocal micro-Raman spectrograph. The excitation source used was the 514.5 nm wavelength line from a Coherent model 70C5 Ar^+ laser operating at a power of 100 mW. A 100-fold objective lens was used for the focusing so that only a volume of 1 µm^3 was sampled. The data were collected for 120 s. The wavenumber resolution is approximately 1 cm^{-1}.

Scanning Electron Microscopy. Micrographs were recorded by means of a ZEISS Supra 55VP scanning electron microscope operating in high vacuum at 3 kV using secondary electron detector (Everhart-Thornley detector). Specimens were prepared by sticking powder onto the surface of an adhesive carbon film.

Small Angle X-Ray Scattering. SAXS measurements of $Y_{2.55}Eu_{0.45}BO_6$ powder and derived composite films were performed under vacuum ambient with a NanoStar System from Bruker instruments. The X-ray was supplied by a Cu cathode, at a wavelength of 1.5418 Å, and then collimated by a Gobel mirror followed by three pinholes. The sample-to-detector distance was 648 mm. The scattering data were collected by a two-dimensional position-sensitive gas detector (HiSTAR) with the scattering vector, $q = 4\pi\sin\theta/\lambda$, ranging from 0.014 Å^{-1} to 0.35 Å^{-1}, using 2θ as the scattering angle.

Luminescence. Absolute photoluminescence (PL) quantum yields and emission features of all powders were measured using C9920-02G PL-QY measurement system from Hamamatsu. The setup comprises a 150W monochromatized Xe lamp, an integrating sphere (Spectralon® Coating, Ø = 3.3 inch) and a high

sensitivity CCD spectrometer for detecting the whole spectral luminescence. The automatically controlled excitation wavelength range spread from 250 nm to 950 nm with a resolution bandwidth better than 5 nm.

Composite luminescence experiments were performed on a Jobin-Yvon set-up consisting of a Xe lamp operating at 400 W and two monochromators (Triax 550 and Triax 180) combined with a cryogenically cold charge coupled device (CCD) camera (Jobin-Yvon Symphony LN2 series) for emission spectra and with a Hamamatsu 980 photomultiplicator for excitation ones.

Luminescence decays were measured at room temperature using the set-up already described[11-12]. The output dye laser is doubled by the mean of DCC1-KDP crystal and spatially dispersed through a Pellin-Broca prism. The dye solution was Rhodamine 590. The UV doubled beam is filtered by UV-UG11 Schott filter and focused on the sample. The fluorescence is selected at right angle from the excitation and analyzed with numerical oscilloscope LeCroy 1GHz-wave Runner.

All luminescence spectra have been recorded at room temperature and corrected from the set-up response.

Results and Discussion

Powders characterizations

Powder X-Ray diffraction

Undoped Y_3BO_6 xerogel crystallization was analyzed by means of HTXRD. The resulting patterns are gathered in Fig. 1.

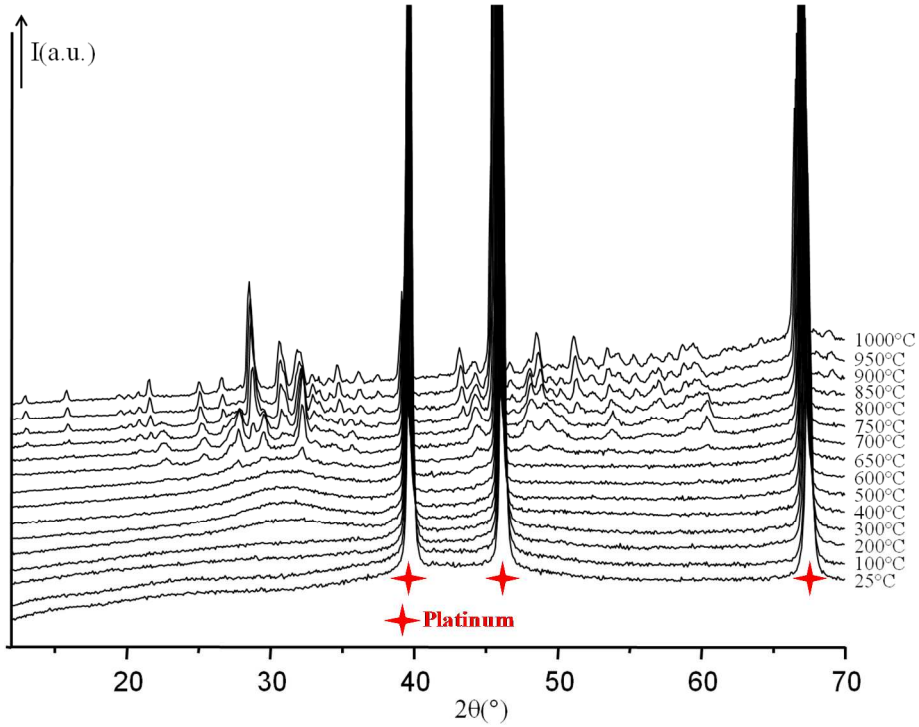

Fig. 1 HTXRD patterns of undoped Y_3BO_6 xerogel

They reveal that Y_3BO_6 begins to crystallize from 700°C and that the crystallization process becomes much more significant at higher temperature since diffraction peaks are much sharper and well defined. After cooling at room temperature, the experimental XRD pattern (Fig. 2) reveals that powder corresponds to nearly pure and well crystallized Y_3BO_6 (ICSD file 84966) phase with a little fraction of Y_2O_3.

On the basis of this study, we have decided to preheat the undoped and doped xerogel at 400°C for 2 hours in air atmosphere in order to minimize the apparition of Y_2O_3 phase; samples were then grounded again and a 4 hours heat-treatment at 1000°C in air was realized. Fig. 3 gathers experimental XRD patterns of the Y_3BO_6:Eu^{3+} (x mol %) powders obtained for x = 1 to 20 mol%. This figure also presents the simulated XRD pattern for Y_3BO_6 plotted from the crystallographic data (ICSD file 84966).

It can be noticed that only pure Y_3BO_6 phases are obtained whatever the Eu^{3+} concentration. No unexpected phase, such as Y_2O_3, has been observed. A shift of the diffraction peaks is observed especially for the most intense one located at around 29° (insert in Fig. 3). The increase of the doping amount leads to an offset of diffraction lines to lower 2 theta values. This observation is in good agreement with the Vegard's law.

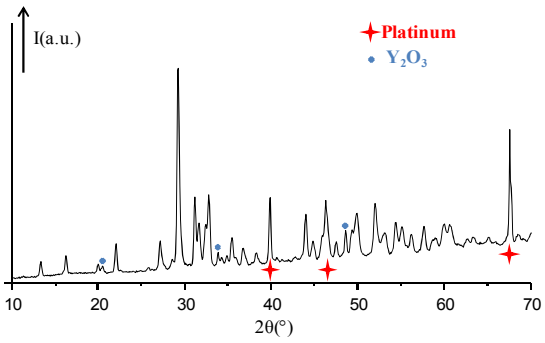

Fig. 2 Room-temperature XRD pattern recorded for undoped Y_3BO_6 xerogel which has undergone the HTXRD program

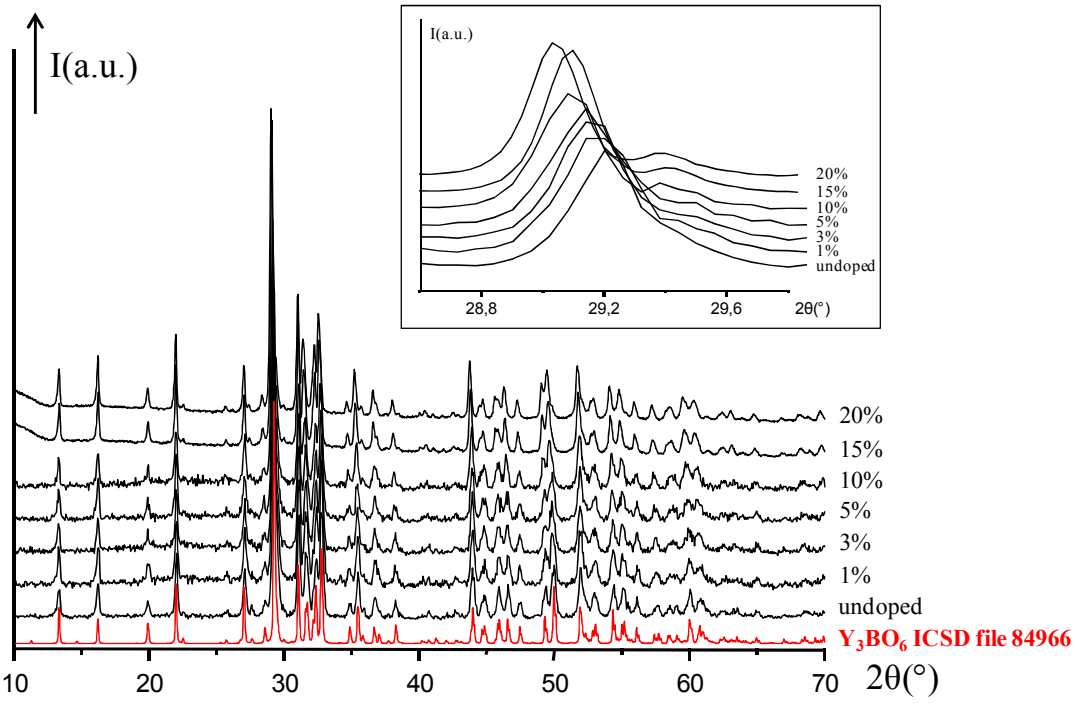

Fig. 3 XRD patterns of the $Y_3BO_6:Eu^{3+}$ (x mol %) powders obtained for x = 1 to 20 mol% and the simulated XRD pattern for Y_3BO_6

Thermal behavior

TG and DTA curves were recorded on both undoped and 1mol% doped xerogels so as to investigate the thermal decomposition process of the Pechini derived Y_3BO_6 powders. Results reported in Fig. 4 indicate the same behavior for both xerogels, with a total weight loss of about 70%. The weight losses occurring below 600°C can be attributed to the removal of absorbed moisture but also to the burning of organic synthesis reagents (chelating and cross-linking reagents) and departure of residual solvents (water and ethanol). Above 600°C, only a weak weight loss takes place, ascribed to the departure of the remaining organic residues which are embedded in Y_3BO_6 matrix. Besides, the exothermic peak located at 780°C corresponds to the onset of Y_3BO_6 crystallization. No significant weight loss is observed subsequently; as a result it is assumed that the final product was obtained i.e. Y_3BO_6 as confirmed by the HTXRD results.

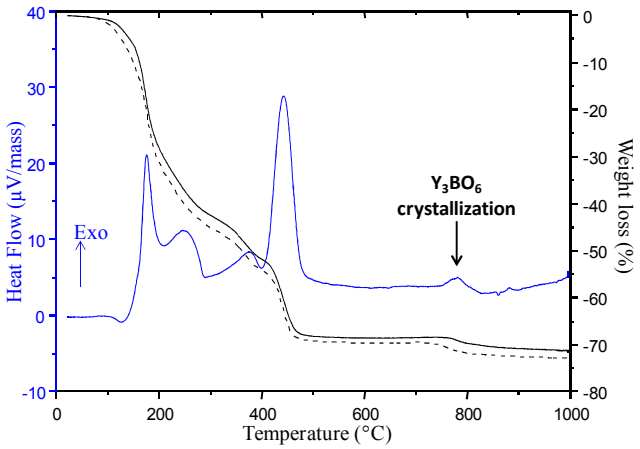

Fig. 4 TG and DTA curves obtained from undoped Y_3BO_6 xerogel (solid lines) and $Y_{2.97}Eu_{0.03}BO_6$ xerogel (dash line)

Infrared and Raman study

FTIR spectra recorded from the undoped Y_3BO_6 xerogel and after sintering at 1000°C for 4 hours are compared in Fig. 5.

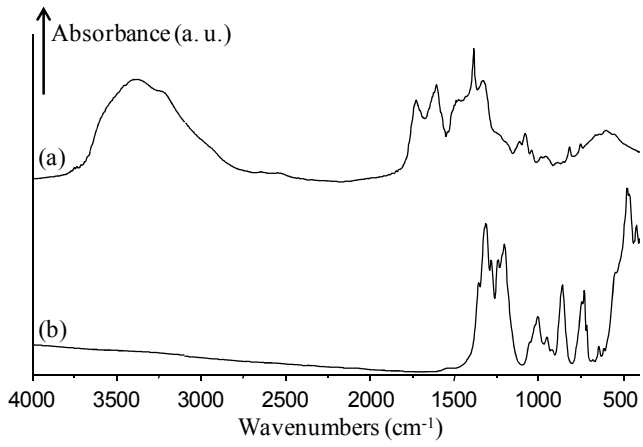

Fig. 5 Infrared spectra recorded from the undoped Y_3BO_6 (a) xerogel and (b) after sintering at 1000°C

For xerogel, the presence of characteristic organic bands is evidenced (Fig. 5a). The broad band ranging from 2700 to 3900 cm^{-1} is consistent with O-H and C-H stretching frequencies coming from the chelating (citric acid) and cross-linking reagents (PEG) as well as residual solvents (water-ethanol). Peaks located at around 1600 and 1720 cm^{-1} correspond both to C=O stretching. Indeed, the band located at 1600 cm^{-1}, which is offset by about 120 cm^{-1} to small wavenumbers compared to free carbonyl groups (~1720 cm^{-1}), can be attributed to C=O function coordinated to a metal cation[17]. After a 4 hour-heating treatment at 1000°C, the IR spectrum (Fig. 5b) is characterized by the disappearance of these organic bands. Such a result is in good

agreement with TG analysis which has shown that the residual organic groups are removed below 600°C. Moreover, the bands observed within the 1600–400 cm^{-1} region are mainly assigned to B–O group vibrations in Y_3BO_6 lattice and are ascribed to the BO_3^{3-} and $B_2O_5^{4-}$ groups. Indeed, according to the literature[9], it was assumed that the yttrium borate known with the formulation Y_3BO_6 corresponds actually to the formula $Y_{17,33}(BO_3)_4(B_2O_5)_2O_{16}$. The structure consists of BO_3^{3-} and $B_2O_5^{4-}$ borate groups as well as seven and eightfold coordinated yttrium atoms.

Raman spectroscopy was also carried out in order to confirm this formula. Fig. 6 presents Raman spectrum of the undoped sample after sintering at 1000°C.

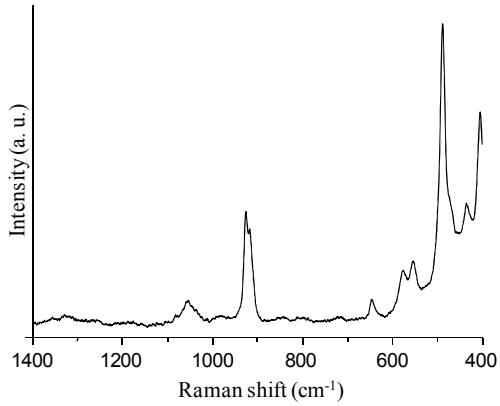

Fig. 6 Raman spectrum of the undoped sample after sintering at 1000°C

Several peaks are observed within the 1400-400 cm^{-1} region. Once again, our results are in good agreement with Lin. *et al.*[9] ones: peaks can be attributed to B–O vibrations in BO_3^{3-} and $B_2O_5^{4-}$ groups in the lattice.

Morphological study

Fig. 7 shows the SEM images of $Y_{2.55}Eu_{0.45}BO_6$ powder. This sample exhibits small grains highly friable which is a key point in order to elaborate composite films embedding this phosphor. The main advantage arises from the ability to grind easily Pechini powder in fine particles suitable for preparing thick or thin luminescent films from phosphors suspension[10].

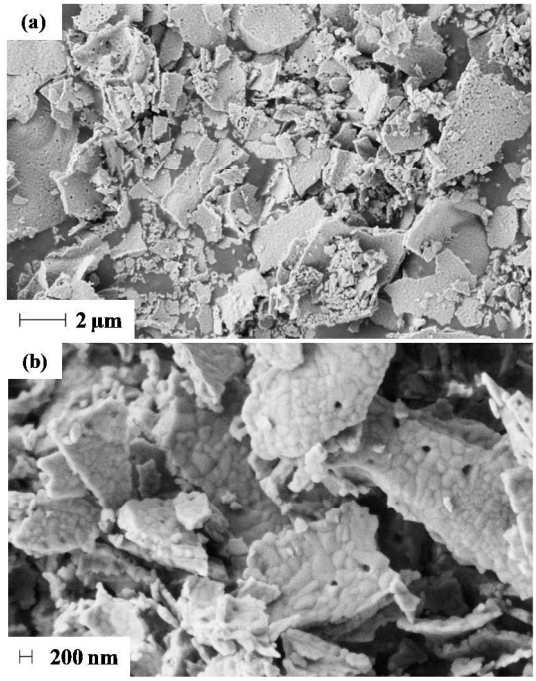

Fig. 7 SEM images (a) x5000 and (b) x20000 of $Y_{2.55}Eu_{0.45}BO_6$ powder

Luminescence properties

Absolute PL quantum yields of Y_3BO_6:Eu^{3+}(x mol %; x = 1 to 20 mol%) powders have been recorded upon excitation in the 250-500 nm range and are presented in Fig. 8.

All spectra show similar features with several excitation bands: they are constituted of a wide band centered at about 270 nm and several sharp peaks at longer wavelengths. The broad band located between 250 and 300 nm is attributed to the Eu^{3+}-O^{2-} charge transfer (CT) band whereas the peaks above 300 nm are assigned to the intra-configurational (f-f) transitions of Eu^{3+} connecting the $^7F_0$ ground state to ^5F_J (320 nm), $^5D_4$ (364 nm), ^5G_J (382 nm), $^5L_6$ (395 nm), $^5D_3$ (415 nm) and $^5D_2$ (466 nm) excited states[10, 18].

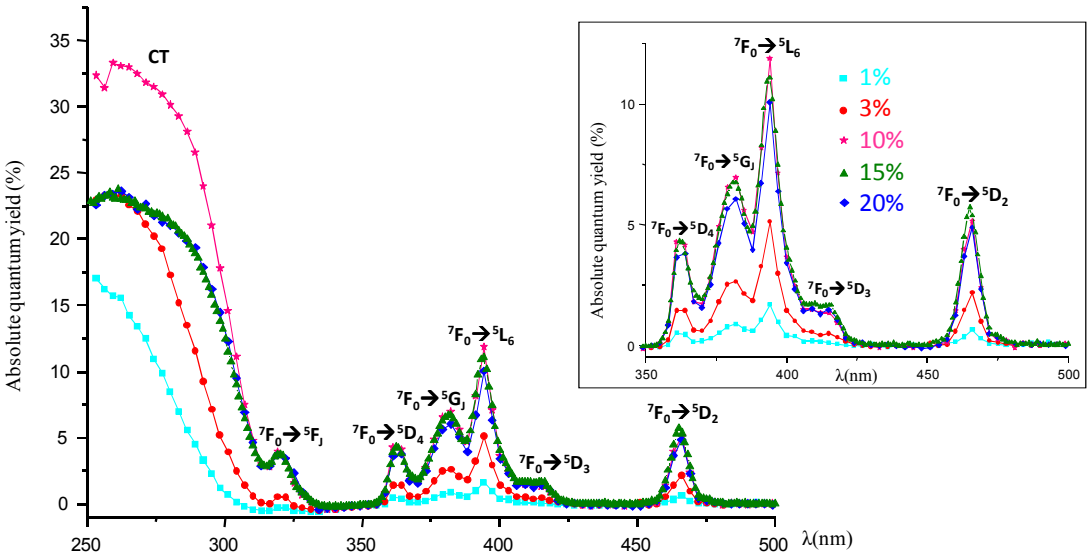

Fig. 8 Evolution of the absolute PL quantum yield for $Y_{3-x}Eu_xBO_6$ powders, in function of the excitation wavelength and recorded at room-temperature

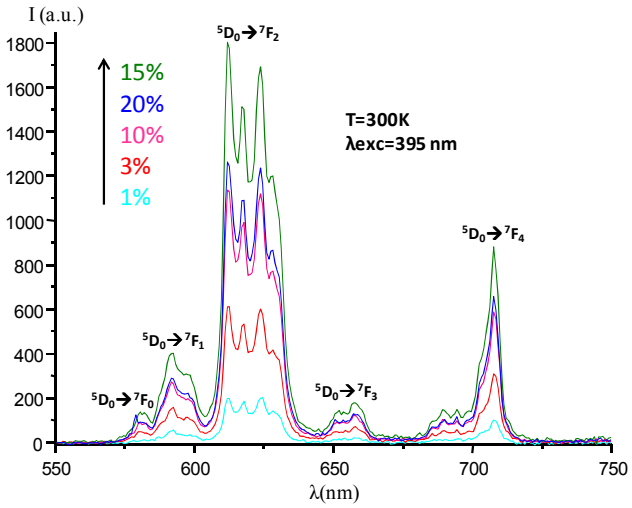

Fig. 9 Room-temperature emission spectra of $Y_{3-x}Eu_xBO_6$ powders upon a 395 nm excitation

Regarding the 395 nm ($^5L_6$) excited emission spectra (Fig. 9), the same profile can be identified for each doping rate with the typical Eu^{3+} emission due to the electronic transitions from $^5D_0$ to the ^7F_J levels (J=0-4). The most intense band located around 620 nm is attributed to the $^5D_0 \rightarrow {}^7F_2$ electric dipole transition[12]. The spectral profile presents relatively large emission bands; such spectral repartition reflect the multisite character of the host, indeed, in the $Y_{17.33}(BO_3)_4(B_2O_5)_2O_{16}$ structure, yttrium ions occupy nine non centro-symmetric independent crystallographic positions[9]. Eu^{3+} ions, that replace Y^{3+} ions, are randomly distributed in these sites, entailing a broadening of the emission bands and several $^5D_0 \rightarrow {}^7F_2$ transitions. Because of the europium multiple sites character in Y_3BO_6 matrix, it is not possible to separate the transitions at ambient temperature and even at low temperature it would remain tricky to do it.

The concentration dependence of the Eu^{3+} emission intensity can be determined: this latter increases with the doping concentration up to about 15 mol% and then declines. This high quenching concentration (15 mol%) is the same as that observed for solid-state reaction[9]. To conclude, 15 mol% has been determined as the optimal concentration leading to the best optical properties upon UV radiation.

Composite characterizations

Fig. 10 shows pictures of the as-synthesized $Y_{2.55}Eu_{0.45}BO_6$ powder (Fig. 10a) and of a thick flexible PVP/$Y_{2.55}Eu_{0.45}BO_6$ composite film with a 28µm thickness (Fig. 10b), both revealing a strong red luminescence upon a 254 nm excitation.

Characterizations presented thereafter have been performed in order to study the influence of shaping on structural properties of phosphors but also to investigate the effect of $Y_{2.55}Eu_{0.45}BO_6$ particles on PVP photostability and to finish, for examining the impact of photoageing on composites optical properties. Indeed, to develop efficient luminescent composite suitable for optical devices, structural and optical properties of the fillers should not change after shaping and incorporation into the polymer matrix.

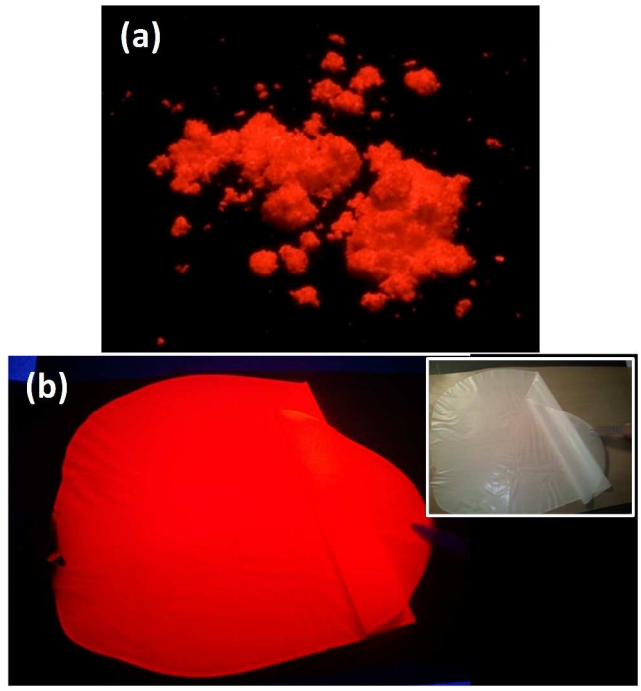

Fig. 10 Pictures of (a) as-synthesized $Y_{2.55}Eu_{0.45}BO_6$ powder and (b) PVP/$Y_{2.55}Eu_{0.45}BO_6$ composite film under excitation at 254nm (daylight in insert)

Structural characterizations

In order to prove that the incorporation of Y_3BO_6:Eu^{3+} powder into a polymeric matrix such as PVP does not lead to structural modifications of the phosphor, an XRD study was performed on the composite film. Resulting patterns obtained for neat PVP and PVP/Y_3BO_6:Eu^{3+} composite films, as well as for the Y_3BO_6:Eu^{3+} powder are gathered in Fig. 11.

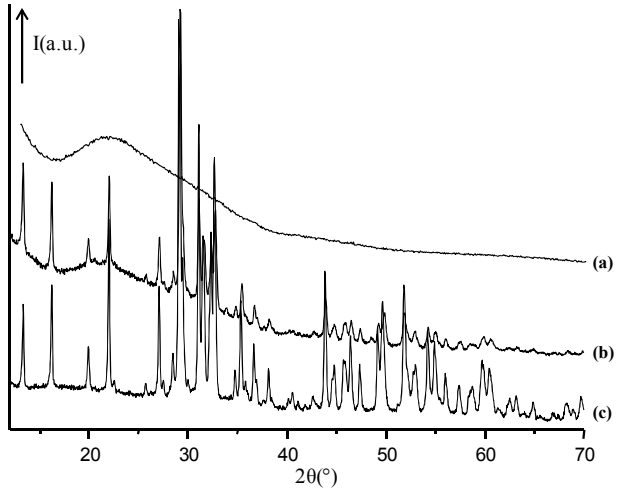

Fig. 11 XRD patterns of PVP film (a), composite film (b) and red phosphor (c)

The neat PVP film presents an amorphous character: it does not exhibit diffraction peaks but only a broad band located around 22° (2θ) (Fig. 11a). The pattern corresponding to the composite film (Fig. 11b) exhibits the most intense diffraction peaks corresponding to Y_3BO_6 structure together with the broad band relative to the polymer matrix.

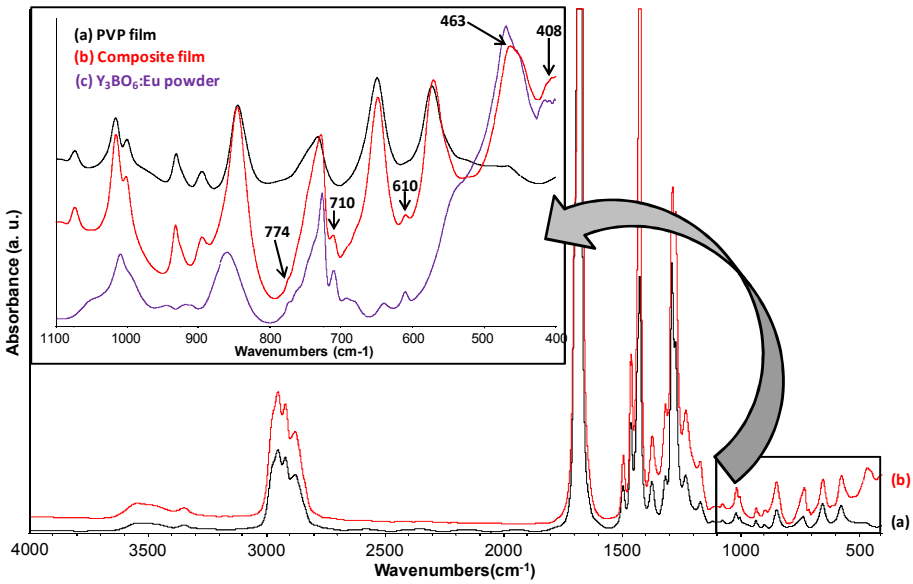

Fig. 12 FTIR spectra of (a) PVP film and (b) PVP/ $Y_{2.55}Eu_{0.45}BO_6$ composite film (a comparison between $Y_{2.55}Eu_{0.45}BO_6$ powder and composite film is shown in insert)

Fig. 12 exhibits a comparison between infrared spectra of a PVP film (Fig. 12a) and a PVP/Y_3BO_6:Eu^{3+} composite film (Fig. 12b). The IR spectrum of the PVP film (Fig. 12a) shows the characteristic absorption bands of PVP[15]. The IR spectrum of the composite film (Fig. 12b) is constituted of the summation of the characteristic IR absorption bands of PVP and Y_3BO_6:Eu^{3+} powder that presents four vibration bands characteristic of Y_3BO_6 structure located at 408, 463, 610 and 710 cm^{-1} as observed on the IR spectrum of Y_3BO_6:Eu^{3+} initial powder (insert in Fig. 12c). Moreover, it can be observed one shouldering at 774 cm^{-1} on the composite IR spectrum also linked to the presence of phosphor fillers.

Luminescence properties

Fig. 13 shows the 395 nm (Eu^{3+}-$^5L_6$) excited emission and 610 nm (Eu^{3+}-$^5D_0$→$^7F_2$) monitored excitation spectra measured at room temperature for starting $Y_{2.55}Eu_{0.45}BO_6$ powder and the same powder embedded in the PVP matrix (PVP/$Y_{2.55}Eu_{0.45}BO_6$ composite film). The emission spectra have been presented with a small offset for clarity while the excitation spectra have been normalized to the O^{2-}→Eu^{3+} CT band for comparison.

The emission spectra of the powder and the composite film are clearly identical indicating that the PVP don't give rise to any modification or contribution in the emission spectral repartition. Indeed the PVP film alone does not show any emission band with an excitation fixed in the overall whole wavelength range of the $Y_{2.55}Eu_{0.45}BO_6$ powder excitation spectra. From Fig. 13 it can be noted that the relative intensity ratio of the CT to 4f-4f transitions of Eu^{3+} drastically increases for the composite sample. In fact, for the powder ($Y_{2.55}Eu_{0.45}BO_6$) this ratio is 0.6 (for instance for CT/$^7F_0$→$^5L_6$) whereas for the composite film (PVP/$Y_{2.55}Eu_{0.45}BO_6$) it results to be 10.9.

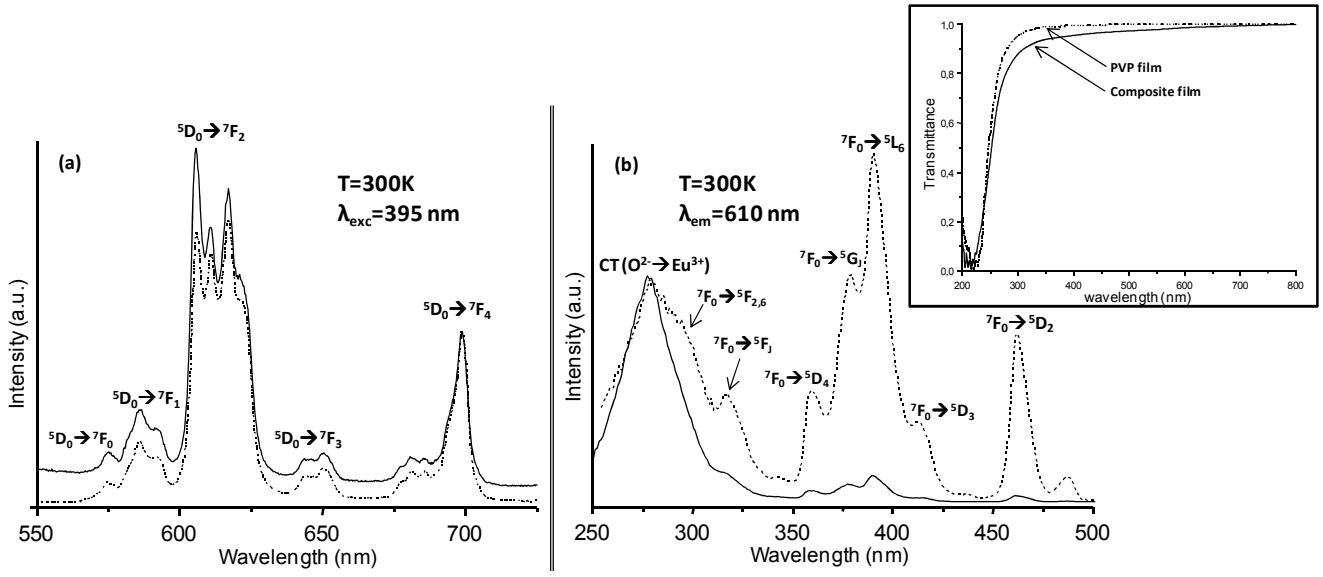

Fig. 13 Room-temperature emission (a) and excitation (b) spectra of the as-synthesized red phosphor (dotted lines) and of the PVP/$Y_{2.55}Eu_{0.45}BO_6$ composite film (solid lines) (Optical transmittance spectra of the PVP film and composite film are shown in insert)

The enhancement of the CT band intensity relative to f-f transition intensities has been already observed for several polymer composites embedding Eu^{3+}-doped inorganic charges[19]. This phenomenon has been explained in term of significant increase of the refractive index of PVP at high energy side of CT band. Indeed, it is well known that the intensities of CT and f-f electronic transitions are strongly dependent on the refractive index of host material[20]. Since the optical properties of the grain powder can be affected by the external host, it is necessary to define a new macroscopic parameter, called the effective refractive index η_{eff}, which can be approximated by a simple model[20]: $\eta_{eff}(X) = X\,\eta_{mat} + (1\text{-}X)\,\eta_{med}$ where η_{mat} is the refractive index of powder, η_{med} is the refractive index of medium and X is the so-called filling factor.

Optical transparency of the composite film is compared with that of the pure PVP film (insert of Fig. 13). Pure PVP film exhibits a transmittance above 99% at the wavelength range 400-800 nm and shows a transmittance which decrease gradually from 99 to 54% between 400 and 250 nm. The transmittance of the composite is slightly affected, however we can note that the decrease of the transmittance is between 95% at 400 nm and 43% at 250 nm. For these reasons, the luminescence decays were measured at room temperature for the $^5D_0 \rightarrow {}^7F_2$ emission band (at ~610 nm) under laser pulsed excitation in the CT band at 280 nm.

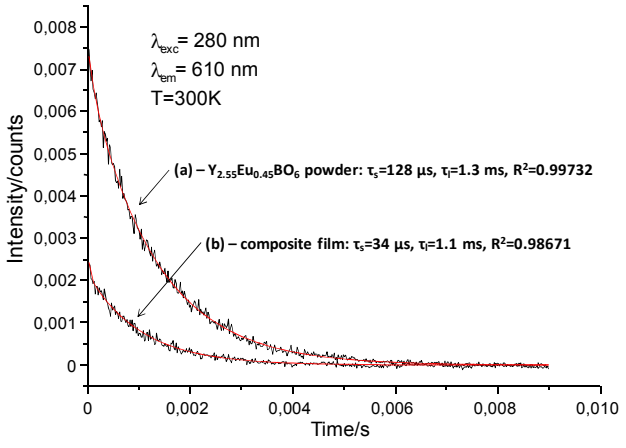

Fig. 14 Decay curves for the $^5D_0 \rightarrow {}^7F_2$ transition of the Eu^{3+} ions in the as-synthesized red phosphor (a) and in the PVP/$Y_{2.55}Eu_{0.45}BO_6$ composite film (b) collected upon a 280 nm excitation at 300 K

The luminescence decays of both powder and composite film (Fig. 14) deviate slightly from pure exponential indicating that they reflect the multisite character of the Eu^{3+} ions embedded in Y_3BO_6 in addition of inter-site energy transfer. Since such analysis is not the subject of this paper, we have determined the effective luminescence decay times from the following equation[21]: $\tau_{eff} = \int I(t)\,t\,dt / \int I(t)\,dt$. The values of τ_{eff} is 1.3 ms for the powder and the composite film, indicating that the global Eu^{3+} fluorescence lies in the same temporal range for both powder and composite film. However two decay time constants can be obtained by a bi-exponential fitting for the powder and composite film (Fig. 14). The value derived for the samples are: τ_s=128 µs and τ_l=1.3 ms for the powder and τ_s=34 µs and τ_l=1.1 ms for the composite film with an intensity contribution of the τ_s of 8.4% and 21% in the global intensity of respectively powder and composite film. This means that the short component of the decays is much affected by the presence of the surrounding PVP. Since the long component τ_l is close to the τ_{eff} for both the powder and the composite film, we can suppose that the decrease of the short component τ_s obtained for the composite film is most probably due to an increase of the effective refractive index, as the refractive index of PVP is higher than in air.

Recent work[22] has shown that the refractive index of pure PVP increases close to exponentially from 1.48 to 1.57 between 400 and 250 nm, confirming that the effective refractive index can play an important role in this range of wavelength. We plane to measure the refractive index of the composite film using for such purpose a spectroscopic ellipsometry, with modifying the $Y_{2.55}Eu_{0.45}BO_6$ phosphor loading rate in the PVP matrix.

Photooxidation of PVP/ Y_3BO_6:Eu^{3+} composite at long wavelengths (λ>300 nm)

A study of the photostability of PVP/$Y_{2.55}Eu_{0.45}BO_6$ films was carried out by comparing structural and optical features of irradiated films (submitted to a maximum of 80 hours of irradiation, λ>300 nm, 60°C) and initial ones. Modifications of the PVP/$Y_{2.55}Eu_{0.45}BO_6$ composite film were first analyzed by transmittance-IR spectroscopy depending on the irradiation time (Fig. 15).

The characteristic IR absorption bands of pristine PVP have been previously described[15]. Photooxidation results in noticeable modifications in the IR spectrum of the composite. In the carbonyl region (Fig. 15a), a band with an absorption maximum at 1770 cm^{-1} appears. The initial amide band centered at 1680 cm^{-1} (Fig. 12) becomes wider and a shoulder at 1735 cm^{-1} can be observed. Moreover, a broad band centered at 1540 cm^{-1} develops. Fig. 15b shows that, in the domain between 1100 and 700 cm^{-1}, new absorption bands develop at 1060, 985, 910, 820 and 785 cm^{-1} during irradiation. One can particularly notice that the decrease in the absorption bands at 845 and 930 cm^{-1} is related to the formation of new absorption bands at 820 and 910 cm^{-1}, respectively, with two isobestic points at 830 and 925 cm^{-1}. These several formed bands correspond to characteristic absorption bands of photoproducts of PVP based on the mechanism of photooxidation that was previously proposed by Hassouna *et al.*[15]. These photoproducts were mainly identified as succinimide groups and vinyl unsaturations. As a result, we can assume that $Y_{2.55}Eu_{0.45}BO_6$ particles have no influence on the photooxidation mechanism of PVP submitted to irradiation at λ>300 nm (T=60°C) since the same photoproducts were obtained. Moreover, the vibration bands characteristics of Y_3BO_6 structure, located at 408, 463, 610, 710 and 774 cm^{-1}, do not evolve during aging.

Kinetic curves of photooxidation for PVP/ Y_3BO_6:Eu^{3+} composite

The influence of $Y_{2.55}Eu_{0.45}BO_6$ particles on the kinetic rate of PVP photooxidation was characterized by IR spectroscopy. The increase in absorbance at 1770, 1060 and 985 cm^{-1} was plotted as a function of irradiation time for composite film and compared with that obtained for pristine PVP irradiated in the same conditions (see Fig 16).

These curves show photoproducts formation from the beginning of irradiation without any induction time. The comparison between composite and pristine PVP kinetic curves of photooxidation does not show important differences. These results allow us to conclude that luminescent $Y_{2.55}Eu_{0.45}BO_6$

particles have no significant influence on the polymer oxidation rate under irradiation at λ > 300 nm at 60°C. In particular, the $Y_{2.55}Eu_{0.45}BO_6$ particles have no prodegrading effect on PVP photooxidation.

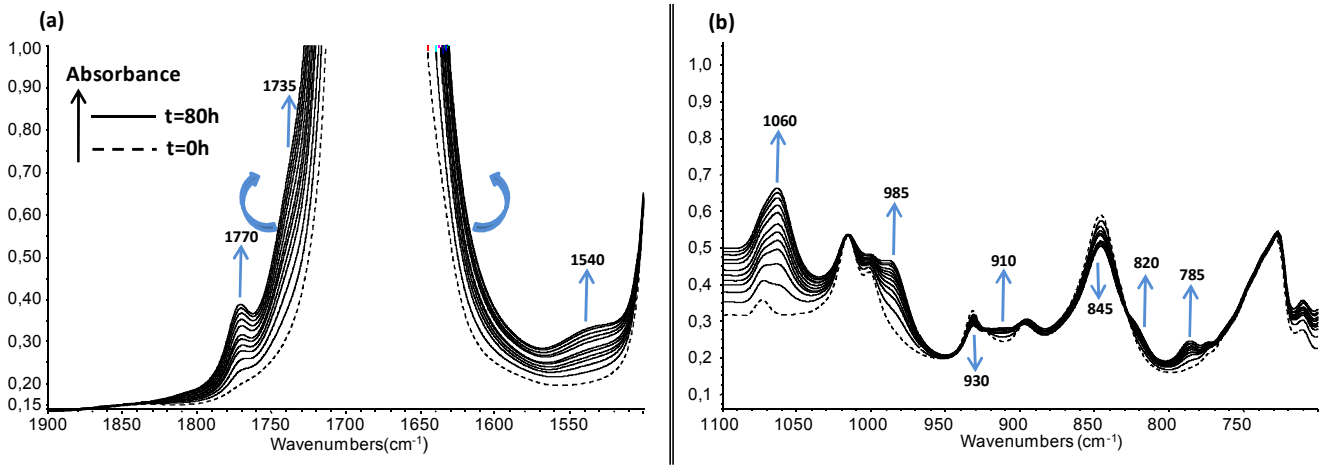

Fig. 15 FTIR spectra of PVP/$Y_{2.55}Eu_{0.45}BO_6$ composite film photooxidized at λ>300 nm and 60°C (a) in the domain 1900-1500 cm^{-1} and (b) in the domain 1100-700 cm^{-1}

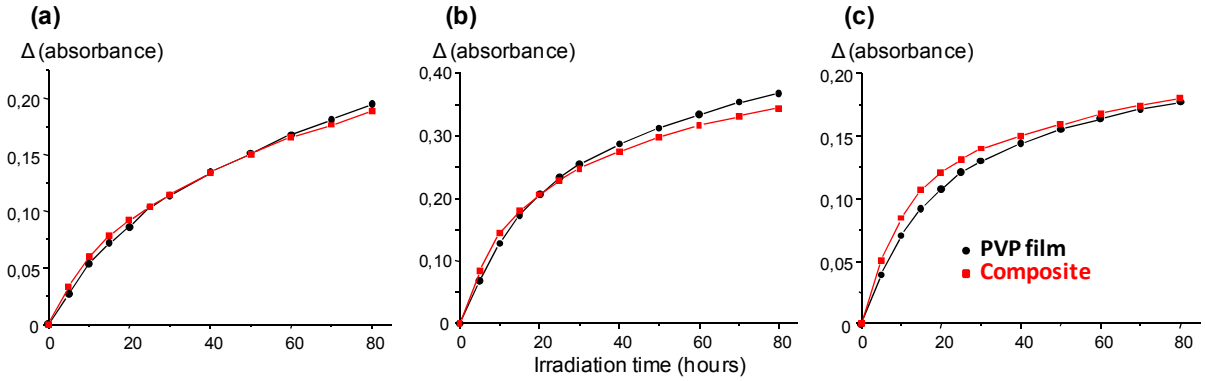

Fig. 16 Kinetic curves of photooxidation for PVP film and PVP/$Y_{2.55}Eu_{0.45}BO_6$ composite film (a) 1770 cm^{-1}, (b) 1060 cm^{-1} and (c) 985 cm^{-1}

Influence of polymer photoaging on $Y_3BO_6:Eu^{3+}$ morphological and optical properties

The effect of PVP photoageing on the structural features of the $Y_3BO_6:Eu^{3+}$ particles present in the pristine powder and in the PVP/$Y_{2.55}Eu_{0.45}BO_6$ composite was evaluated from the comparison between the SAXS curves gathered on the log-log plot displayed in Fig. 17. All patterns are characterized by a single linear function covering the q-range between 0.01 and 0.1 $Å^{-1}$. This behavior demonstrates that both the $Y_3BO_6:Eu^{3+}$ powder and the composite film obey the Porod law ($I(q) \propto q^{-4}$) expected for a two-electronic density model of bi-phase material with sharp and smooth interface[23]. The wide range of validity of the Porod law confirms that the studied samples structure just consist of a particles dispersion into a homogeneous matrix. Moreover the linear behavior of the SAXS curve is essentially unaffected after photoageing, indicating that the structure of the interface between the $Y_{2.55}Eu_{0.45}BO_6$ particles and the matrix is not damaged by the photo-irradiation. This comportment is different from that previously observed on a PVP/$BaMgAl_{10}O_{17}:Eu^{2+}$ composite[24] for which a slightly rough interface between the particles and the polymer matrix is observed. In this case, photoaging leads to the apparition of another interface and increases the interface roughness between particles and polymer matrix.

The effect of PVP photoageing on the luminescence efficiency was also investigated. Optical features of composite film were recorded before and after irradiation for 80 hours: excitation and emission spectra are gathered in Fig. 18.

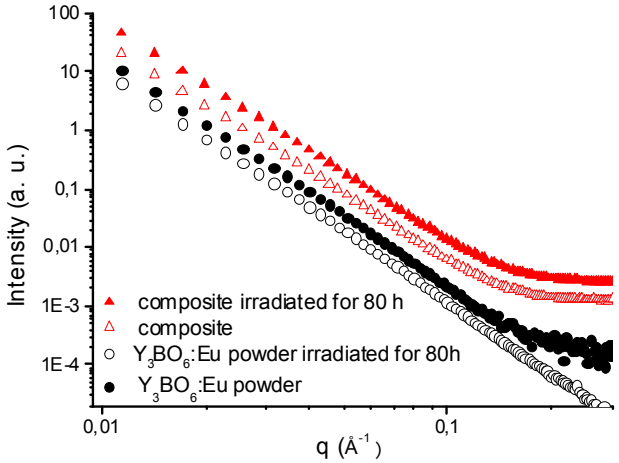

Fig. 17 Log-log plot of SAXS intensity, I(q), as a function of the scattering vector, q, for $Y_{2.55}Eu_{0.45}BO_6$ powder and PVP/$Y_{2.55}Eu_{0.45}BO_6$ composite film before and after 80h of irradiation (λ>300 nm, T=60°C). The curves were vertically shifted for clarity.

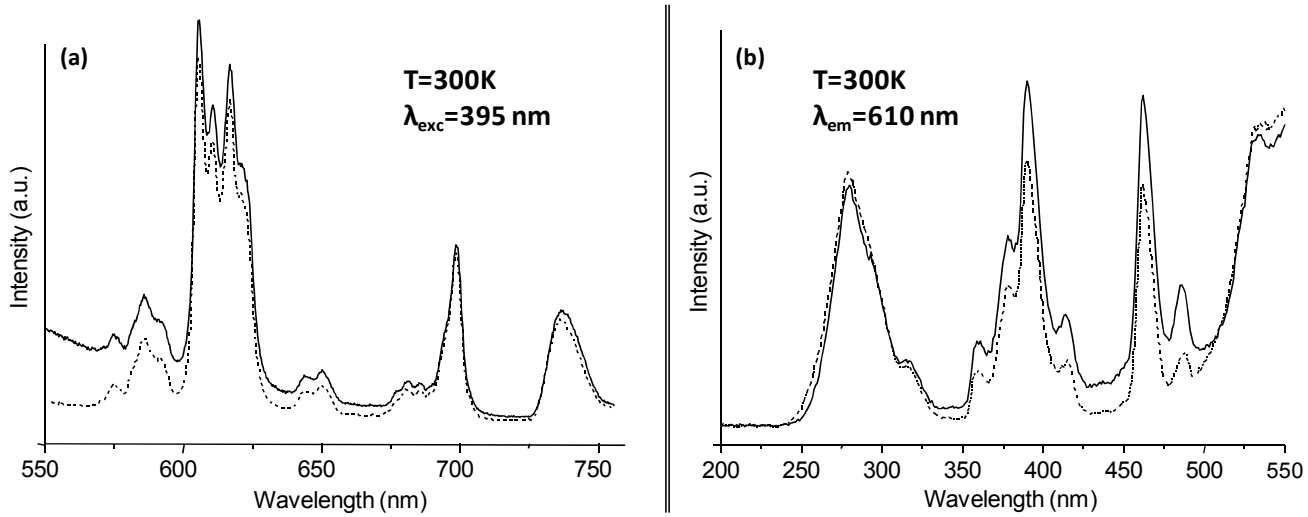

Fig. 18 Room-temperature emission (a) and excitation (b) spectra of the PVP/$Y_{2.55}Eu_{0.45}BO_6$ composite film depending on the irradiation time: at the initial state (dotted lines) and after 80 hours of irradiation (solid lines)

Overall, spectra have the same profile. Concerning excitation spectra (Fig. 18b), composite photooxidation did not modify neither Eu^{3+} absorption band position nor Eu^{3+}-O^{2-} CT band. On the other hand, concerning the emission properties (Fig. 18a), no real modification was observed.

Conclusion

Red luminescent, flexible and thick PVP/Y_3BO_6:Eu^{3+} composite film has been easily elaborated from crystallized powder, synthesized by Pechini method and dispersed in a PVP alcoholic solution. Synthesized powder, thanks to its optical properties, revealed to be a promising candidate as phosphor for near UV-LEDs based lighting devices. The best doping rate of Eu^{3+} in the matrix was determined to be 15 mol%. This synthesized powder is highly friable and thus easily grinded into fine particles, to be homogeneously dispersed into a PVP polymer solution to make a luminescent composite suspension. Shaping as composite films did not modify structural and optical features of the as-synthesized red phosphor. However, it was found that the CT band intensity observed for the composite film is strongly enhanced with respect to the powder one. This phenomenon is discussed in the framework of already published results considering strong enhancement of the refractive index of PVP matrix in the energy range of CT band. Moreover, photoageing experiments have demonstrated that the presence of Y_3BO_6:Eu^{3+} particles did not influence the photodegradation mechanism of the polymer matrix and that they were not prodegrading. In the same way, irradiation at wavelengths higher than 300 nm does not modify the fluorescence emission of PVP/Y_3BO_6:Eu^{3+} composite. Nowadays, the photostability is a key point for LEDs marketing in order to develop a complete product sheet characterizing devices durability. Composite films could be associated with an excitation source, such as near UV LED, to produce colored or white light (after combination with other phosphors).

Acknowledgments

The authors would like to thank Anne-Marie Gélinaud (Casimir, Aubière, France) for her help in acquiring SEM pictures.

Notes and references

[a] *Clermont Université, ENSCCF, Institut de Chimie de Clermont-Ferrand, BP 10448, F-63000 CLERMONT-FERRAND, France*
E-mail: genevieve.chadeyron@ensccf.fr
Fax: +334 73407108 Tel: +334 73407109
[b] *Clermont Université, Université Blaise Pascal, Institut de Chimie de Clermont-Ferrand, BP 10448, F-63000 CLERMONT-FERRAND, France*
[c] *CNRS, UMR 6296, ICCF, BP 80026, F-63171 AUBIERE, France*
[d] *Instituto de Química, UNESP, R. Prof. Francisco Degni 55, 14800-900 Araraquara, SP, Brazil*

1. S. Ye, F. Xiao, Y. X. Pan, Y. Y. Ma and Q. Y. Zhang, *Mater. Sci. Eng., R*, 2010, **71**, 1.
2. E. F. Schubert and J. K. Kim, *Science*, 2005, **308**, 1274.
3. L. Chen, C.-C. Lin, C.-W. Yeh and R.-S. Liu, *Materials*, 2010, **3**, 2172.
4. P. F. Smet, A. B. Parmentier and D. Poelman, *J. Electrochem. Soc.*, 2011, **158**, R37.
5. M. R. Krames, O. B. Shchekin, R. Mueller-Mach, G. O. Mueller, L. Zhou, G. Harbers and M. G. Craford, *J. Disp. Technol.*, 2007, **3**, 160.
6. R. Kasuya, A. Kawano, T. Isobe, H. Kuma and J. Katano, *Appl. Phys. Lett.*, 2007, **91**, 111916.
7. M. L. Saladino, A. Zanotto, D. Chillura Martino, A. Spinella, G. Nasillo and E. Caponetti, *Langmuir*, 2010, **26**, 13442.
8. D. Bera, S. Maslov, L. Qian, J. Soo Yoo and P. H. Holloway, *J. Disp. Technol.*, 2010, **6**, 645.
9. J. H. Lin, S. Zhou, L. Q. Yang, G. Q. Yao, M. Z. Su and L. P. You, *J. Solid State Chem.*, 1997, **134**, 158.
10. G. Chadeyron, N. Pradal, A. Potdevin, D. Boyer, S. Therias, M. Consonni and R. Mahiou, *J. Solid State Sci. Technol.*, 2013, **2**, R3041.
11. G. Chadeyron, R. Mahiou, A. Arbus and J. C. Cousseins, *Eur. J. Sol. State Inor.*, 1997, **34**, 25.

12. D. Boyer, G. Bertrand-Chadeyron, R. Mahiou, A. Brioude and J. Mugnier, *Opt. Mater.*, 2003, **24**, 35.
13. H. Zhu, L. Zhang, T. Zuo, X. Gu, Z. Wang, L. Zhu and K. Yao, *Appl. Surf. Sci.*, 2008, **254**, 6362.
14. X. Liu, F. Zhou, M. Gu, S. Huang, B. Liu and C. Ni, *Opt. Mater.*, 2008, **31**, 126.
15. F. Hassouna, S. Therias, G. Mailhot and J.-L. Gardette, *Polym. Degrad. Stab.*, 2009, **94**, 2257.
16. J. Lemaire, R. Arnaud and J. L. Gardette, *Rev. Gen. Caoutch. Plast.*, 1981, **613**, 87.
17. S. Kureti and W. Weisweiler, *J. Non-Cryst. Solids*, 2002, **303**, 253.
18. N. Pradal, A. Potdevin, G. Chadeyron and R. Mahiou, *Mater. Res. Bull.*, 2011, **46**, 563.
19. D. Hreniak, J. Doskocz, P. GŁuchowski, R. Lisiecki, W. Stręk, N. Vu, D. X. Loc, T. K. Anh, M. Bettinelli and A. Speghini, *J. Lumin.*, 2011, **131**, 473 and the references given therein.
20. R. S. Meltzer, S. P. Feofilov, B. Tissue and H. B. Yuan, *Phys. Rev. B*, 1999, **60**, R14012.
21. E. Nakazawa, in S. Shionoya, *Phosphor Handbook*, ed. W.M. Yen, CRC Press, Boca Raton, FL, USA1999, p. 104.
22. M. H. Ullah, J.-H. Kim and C.-S. Ha, *Mater. Lett.*, 2008, **62**, 2249.
23. G. E. S. Brito, C. V. Santilli, S. H. Pulcinelli and A. F. Craievich, *J. Non-Cryst. Solids*, 1997, **217**, 41.
24. N. Pradal, G. Chadeyron, S. Therias, A. Potdevin, C. V. Santilli and R. Mahiou, *Dalton Trans.*, 2014, **43**, 1072.

Graphical Abstract

The red luminescent composite, achieved by film casting method, proved to be a promising candidate for applications in UV-LEDs based lighting devices.